Comparison of Electromagnetic Induction and Electrical Resistivity Tomography in Assessing Soil Salinity: Insights From Four Plots With Distinct Soil Salinity Levels

Maria Catarina Paz , Nádia Luísa Castanheira , Ana Marta Paz , Maria Conceição Gonçalves , Fernando Monteiro Santos , Mohammad Farzamian *

Posted Date: 9 January 2024

doi: 10.20944/preprints202401.0696.v1

Keywords: electromagnetic induction; electrical resistivity tomography; soil salinity

Article

Comparison of Electromagnetic Induction and Electrical Resistivity Tomography in Assessing Soil Salinity: Insights from Four Plots with Distinct Soil Salinity Levels

Maria Catarina Paz [1], Nádia Luísa Castanheira [2], Ana Marta Paz [2], Maria Conceição Gonçalves [2], Fernando Monteiro Santos [3] and Mohammad Farzamian [2,4,*]

[1] Instituto Politécnico de Setúbal, ESTBarreiro, Rua Américo da Silva Marinho, 2839-001 Lavradio, Portugal
[2] Instituto Nacional de Investigação Agrária e Veterinária, Avenida da República, Quinta do Marquês (edifício sede), 2780-157 Oeiras, Portugal
[3] Instituto Dom Luiz, Faculdade de Ciências da Universidade de Lisboa, Campo Grande, Edifício C1, Piso 1, 1749-016 Lisboa, Portugal
[4] Centre of Geographical Studies (CEG), IGOT, Universidade de Lisboa, 1600-276 Lisbon, Portugal
* Correspondence: Mohammad Farzamian (mohammad.farzamian@iniav.pt)

Abstract: Electromagnetic induction (EMI) and electrical resistivity tomography (ERT) are geophysical techniques measuring soil electrical conductivity, providing insights into properties correlated with it, to depths of several meters. EMI measures apparent electrical conductivity (EC_a, dS m^{-1}) without physical contact, while ERT acquires apparent electrical resistivity (ER_a, ohm m) using electrodes. Both involve mathematical inversion to obtain models of spatial distribution for soil electrical conductivity (σ, mS m^{-1}) and electrical resistivity (ρ, ohm m), respectively, where ρ is the reciprocal of σ. Soil salinity can be assessed from σ over large areas by a calibration process consisting of a regression between σ and the electrical conductivity of the saturated soil paste extract (EC_e, dS m^{-1}), used as a proxy for soil salinity. This research aims to compare the prediction abilities of the faster EMI to the more reliable ERT for estimating σ and predicting soil salinity. The study conducted surveys and sampling at four locations with distinct salinity levels in Portugal, analysing the agreement between the techniques and obtained 2D vertical soil salinity maps. In our case study, the agreement between EMI and ERT models was fairly good in three locations, with σ varying between 50 and 500 mS m^{-1}. However, this was not the case at location 4, where σ exceeded 1000 mS m^{-1} and EMI significantly underestimated σ, when compared to ERT. As for soil salinity prediction, both techniques generally provided satisfactory and comparable regional-level predictions of EC_e, and the observed underestimation in EMI models did not affect significantly the overall estimation of soil salinity. Consequently, EMI demonstrated an acceptable level of accuracy in comparison to ERT in our case studies, supporting the confidence in utilizing this faster and more practical technique for measuring soil salinity over large areas.

Keywords: electromagnetic induction; electrical resistivity tomography; soil salinity

1. Introduction

Electromagnetic induction (EMI) and electrical resistivity tomography (ERT) are two near-surface geophysical techniques that allow to measure the electrical conductivity of soil and therefore to monitor properties that are correlated with it, such as soil salinity (Corwin & Lesch, 2005; Paz et al., 2023; Paz et al., 2020a), soil sodicity (Paz et al., 2020b), soil water content (Shanahan et al., 2015; Whalley et al., 2017), particle size distribution (Huang et al., 2014; Zare et al., 2020; Ramos et al., 2023), and soil cation exchange capacity (Triantafilis et al., 2009; Koganti et al., 2018; Zhao et al., 2020; 2022) to depths that can go up to several meters.

EMI implies the acquisition of apparent electrical conductivity (EC_a, dS m^{-1}) using a device that doesn't touch the surface of the soil, while ERT involves the acquisition of apparent electrical resistivity (ER_a, ohm m), which is the reciprocal of EC_a, using a device that takes measures in

electrodes placed at the surface of the soil. Both EMI and ERT techniques involve the mathematical inversion of the apparent data (Jupp & Vozoff, 1975) to obtain models of the spatial distribution of the soil electrical conductivity (σ, mS m^{-1}), and of the soil electrical resistivity (ρ, ohm m) respectively. Different inversion methods (e.g., Monteiro Santos, 2004; Moghadas, 2019; Narciso et al., 2022) and software (e.g., EMTOMO, 2018; Mclachlan et al., 2021) have been developed to estimate the distribution of σ based on measured EC_a data. Similarly, various inversion codes are available to estimate the distribution of ρ based on measured ER_a data (e.g., Loke, 2002, Rücker et al., 2017; Blanchy et al., 2020). ρ is the reciprocal of σ, so it can be easily converted to σ.

While the fundamental physical principles differ (induction versus galvanic phenomena), and the volume of ground investigated by the two techniques is also different, both could yield similar electrical conductivity values under specific assumptions. Theoretically, adopting low-frequency signals (f < 105 Hz) and the absence of metallic objects in the subsoil should result in comparable outcomes for ERT and EMI techniques. However, it's important to note that ERT is more sensitive to strong resistors, while EMI is more sensitive to strong conductors (Araújo et al., 2023).

Soil salinity can be assessed from σ over large areas by a calibration process consisting of a regression model between σ and the electrical conductivity of the saturated soil paste extract (EC_e, dS m^{-1}), used as a proxy for soil salinity, and conversion of the σ models into salinity maps using the obtained calibration equation (e.g., Koganti et al., 2018; Gómez Flores et al., 2022; Khongnawang et al., 2022; Farzamian et al., 2023). While both EMI and ERT offer non-invasive, rapid, and cost-effective analysis, EMI stands out for its capability to cover extensive areas in a very short timeframe. However, several studies (e.g., Lavoué et al., 2010; Minsley et al., 2012; Moghadas et al., 2017; von Hebel et al., 2014; 2019; Dragonetti et al., 2018; Dragonetti et al., 2022) have highlighted that EMI may not provide precise estimations of σ distribution and may require prior calibration of EC_a data against ERT or time domain reflectometry (TDR) measurements to account for expected shifts and offsets to obtain more representative EC_a measurements. However, the calibration process is site-specific, time-consuming, and may not be feasible in many cases.

In this study, we explore the prediction ability of EMI in assessing soil salinity without prior calibration, comparing the outcomes to equivalent results derived from the ERT data. The aim is to assess whether satisfactory prediction results can be achieved without a prior EMI calibration process. Given that many applications of EMI in soil salinity assessment often skip such calibration step due to its time-consuming nature or the unavailability of necessary geophysical equipment, this case study offers insights into potential uncertainties associated with the absence of calibration. To achieve our goal, we conducted EMI and ERT surveys, along with soil sampling, at four locations with varying salinity levels from non-saline to severely saline soils in the Lezíria de Vila Franca de Xira, an alluvial agricultural area in Portugal. The selection of locations aimed to encompass a range of soil salinity levels, ensuring also great variability of σ, expected when conducting EMI surveys over saline soil across the globe. To this aim, we generated 2D vertical σ models and analysed the agreement between the two techniques in estimating σ at the same subsurface points. Then we obtained one calibration equation for each technique, compared their abilities to predict EC_e from the σ models, and generated 2D vertical soil salinity maps.

2. Study area

The investigation was conducted in Lezíria de Vila Franca, situated 10 kilometers northeast of Lisbon, Portugal (see Figure 1). It is a 130-square-kilometer alluvial peninsula bounded by the Tejo and Sorraia rivers. The climate is classified as temperate with hot and dry summers according to the Köppen classification. In the northern region, the soils exhibit a fine to very fine texture and are categorized as Fluvisols and in the southern region are categorized as Solonchaks, based on the Harmonized World Soil Database (Fischer et al., 2012). There is a gradient of soil salinity that increases from north to south that affects the land use distribution, likely attributed to the regional presence of marine sediments and the saline influence of the estuary on groundwater in the southern part of study area (Ramos et al., 2020). Closer to the estuary in the southern part, tidal variations

Preprints (www.preprints.org) | NOT PEER-REVIEWED | Posted: 9 January 2024 doi:10.20944/preprints202401.0696.v1

influence groundwater depth and salinity. In this area, the land use primarily comprises rainfed pastures, while in the north, there are mainly irrigated annual crops.

For the comparative assessment, four distinct locations with varying salinity levels were selected within the study area (see Figure 1). Location 1 exhibited non-saline conditions (ECe<2 dS m^{-1}), location 2 was slightly saline (2–4 dS m^{-1}), location 3 was moderately to highly saline (4–16 dS m^{-1}), and location 4 was severely saline, surpassing 16 dS m^{-1} at the time of the experiment (Farzamian et al., 2019). During the surveys, location 1 featured drip-irrigated tomatoes, and locations 2 and 3 had maize irrigated by centre pivots, with no irrigation occurring on survey days. Location 4 represented a rainfed spontaneous pasture that had not been ploughed for at least the past decade.

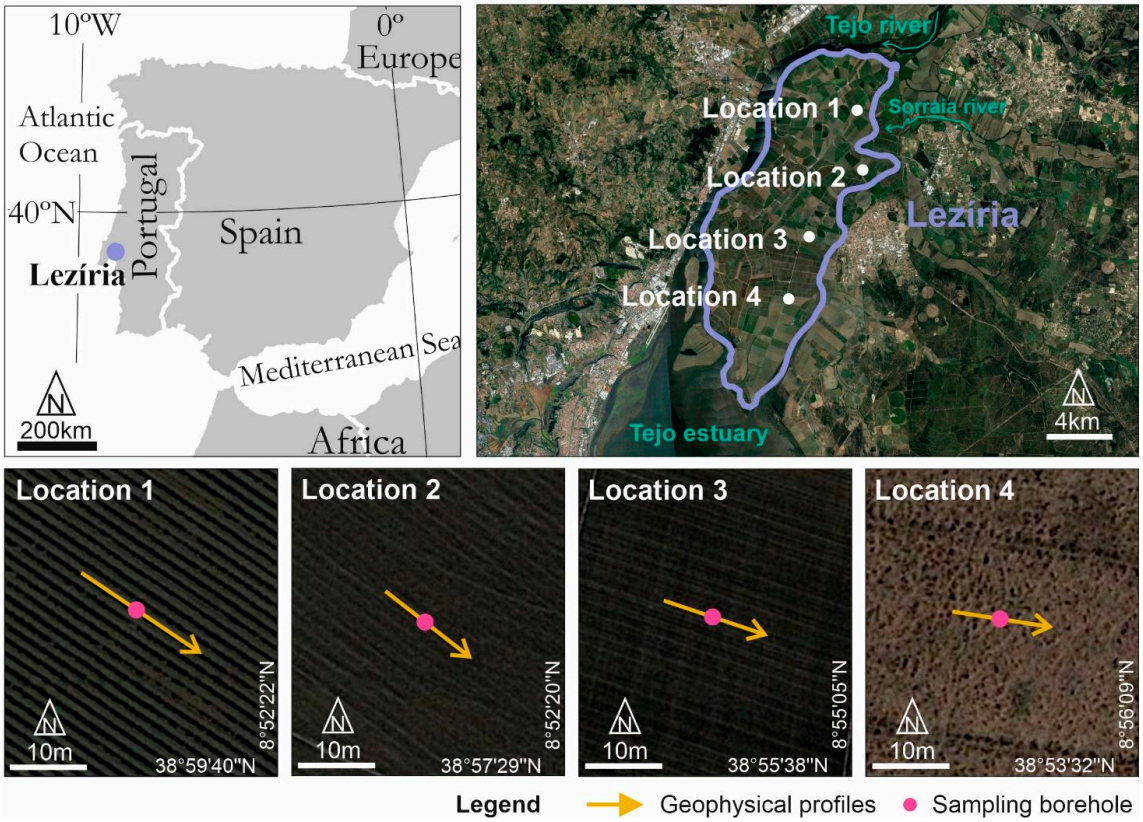

Figure 1. Location of Lezíria, the study area, and details of the four locations with the geophysical transects and soil sampling sites. © Google Earth.

3. Methodology

3.1. Electromagnetic induction

Electromagnetic induction (EMI) data were gathered employing the EM38 instrument. The instrument comprises two coils housed in a case—one for transmitting the electromagnetic signal and the other for receiving it—positioned 1 meter apart. The instrument can be oriented vertically (horizontal dipole mode) for a maximum depth of investigation of 1.5 meters or horizontally (vertical dipole mode) for a maximum depth of 0.75 meters. EMI surveys were conducted in the dry seasons of 2017 (locations 1 and 4) and 2018 (locations 2 and 3). EC_a measurements were collected at 1 m intervals along a 20 m transect at each location (refer to Figure 1) and at two heights from the soil surface (0.15 and 0.4 m) in both horizontal and vertical dipole orientations. This positioning was facilitated by placing the EM38 on a custom-built cart for precision (Farzamian et al., 2019).

The inversion of EC_a data to derive σ was executed using EM4SOIL software (EMTOMO, 2018). The EC_a responses in the model were determined through forward modelling based on the complete solution of the Maxwell equations (Kaufman & Keller, 1984). The subsurface model employed in the inversion consisted of a series of 1-D models distributed according to the EC_a measurement positions.

Preprints (www.preprints.org) | NOT PEER-REVIEWED | Posted: 9 January 2024 doi:10.20944/preprints202401.0696.v1

Each subsurface model at a measurement position was influenced by neighbouring models, enabling algorithm use in regions characterized by high conductivity contrast. The inversion of EC_a data employed an approach grounded in Occam regularization (deGroot-Hedlin & Constable, 1990). Data from all four locations were inverted, applying a five-layer earth initial model with an electrical conductivity of 100 mS m^{-1} and a fixed layer thickness of 0.30 m. The algorithm's parameters, including the inversion algorithm type, number of iterations, and smoothing factor (λ) controlling model roughness, were chosen according to the methodology outlined in (Farzamian et al., 2019). With the evenly distributed inverted data across the modelled area, 2D vertical σ models were generated for each location utilizing triangulation with linear interpolation.

3.2. Electrical Resistivity Tomography

Electrical resistivity tomography (ERT) data was acquired using a 4-point light 10 W system (LIPPMANN, Schaufling, Germany). The technology of this system is based on the measurement of voltage between two reading electrodes installed on the soil surface, when direct current is injected into two other electrodes, to calculate subsurface electrical resistivity. In this system, the disposition of the electrodes changes according to the array used, so that a grid of subsoil ER_a values is obtained. Maximum depth of investigation and resolution vary with electrode spacing and the array configuration. ERT surveys were done at the same transects as EMI surveys, on the same dates, with electrode spacings of 1 m at location 1 and of 0.75 m at locations 2, 3 and 4. ER_a data was collected using the Wenner array, known for effective mapping in areas with significant vertical gradients of σ and a superior signal-to-noise ratio (Loke, 2002).

The inversion of ER_a data to derive σ was performed using RES2DINV software (Geotomo Software, Penang, Malaysia). Given the pronounced vertical salinity gradients due to saline groundwater in the region, robust inversion and mesh refinement to half of the electrode spacing were implemented to address anticipated strong resistivity contrasts. In robust inversion, the objective function aims to minimize the absolute change in resistivity values, yielding models with well-defined interfaces between regions with varying resistivity values (Loke, 2002). Since the inverted data was evenly distributed over the modelled area, 2D vertical σ models were produced for each location using triangulation with linear interpolation.

3.3. Soil salinity

Soil samples were collected at the same time as the geophysical surveys, in the medium point of each profile, as shown in Figure 1. At each sampling site, five soil samples were collected between 0.15 m to 1.35 m depth, as follows: representing topsoil (0–0.3 m), subsurface (0.3–0.6 m), upper subsoil (0.6–0.9 m), intermediate subsoil (0.9–1.2 m), and lower subsoil (1.2–1.5 m).

In the laboratory, EC_e was determined using a conductivity meter (WTW 1C20-0211 inoLab) on extracts obtained from soil saturation paste derived from 300 g of air-dried and 2 mm sieved soil samples. The methodology employed for EC_e measurement followed the procedures by Allison et al. (1954). In this study, soil samples are classified according to EC_e level as non-saline (EC_e<2 dS m^{-1}), slightly saline (2–4 dS m^{-1}), moderately saline (4–8 dS m^{-1}), highly saline (8–16 dS m^{-1}), and severely saline (>16 dS m^{-1}), according to Barrett-Lennard et al. (2008).

Two regional calibrations were developed to predict EC_e from all locations together, one using σ obtained from the inversion of EMI data and the other using σ obtained from inversion of ERT data. The prediction ability of these calibrations was analysed through cross-validation, using the leave-one-out cross-validation in R language (R Core Team, 2020) through the function train(). In this method, one sample is removed and a calibration is established based on the remaining samples to predict the EC_e of the removed sample. This procedure is iteratively repeated for each sample, until all the 19 samples are removed. The prediction ability of the calibrations was evaluated by calculating the root mean square errors (RMSE), and the mean errors (ME). RMSE evaluates matching between measured and predicted data, indicating more precise predictions when closer to zero. ME evaluates whether the predicted data are overestimated (negative ME) or underestimated (positive ME). RMSE and ME were calculated according to the following equations:

Preprints (www.preprints.org) | NOT PEER-REVIEWED | Posted: 9 January 2024 doi:10.20944/preprints202401.0696.v1

$$RMSE = \sqrt{\frac{\sum_{i=1}^{n}(mEC_{e_i} - pEC_{e_i})^2}{n}} \quad (1)$$

$$ME = \frac{\sum_{i=1}^{n}(mEC_{e_i} - pEC_{e_i})}{n} \quad (2)$$

where mEC_e indicates measured EC_e and pEC_e indicates predicted EC_e.

The two regional calibrations were then used to estimate EC_e from σ (either obtained from EMI or ERT). Since the estimated EC_e data was evenly distributed over the mapping area, 2D vertical soil salinity classification maps were produced for each location using triangulation with linear interpolation.

3.4. Agreement analysis

Agreement analysis was performed for EMI and ERT techniques in estimating σ and EC_e on the same points of the subsurface, based on the methodology described in Bland & Altman (1999). In this methodology, the agreement is analysed using the differences between measurements made by two techniques on the same subject. In this study, we considered the subsurface position as the subject. However, both EMI and ERT data surveys and inversion processes produced subsurface σ grids that were not entirely coincident in space (Figure 2). To overcome this issue, σ grids obtained from EMI and ERT modelling results were ordered in data pairs selected for being distanced less than 0.22 m horizontally and 0.05 m vertically. This criterion was looser in the horizontal direction to maintain a statistically significant number of selected points, and it could be accepted because it was known from previous studies (Farzamian et al., 2019; Paz et al., 2020a; b) that the subsurface is highly horizontally stratified. The position attributed to each data pair was the position of the corresponding EMI measurement. These data pairs were then used for comparison of EMI and ERT techniques in estimating σ, represented by (σ_{ERT}, σ_{EMI}).

For comparison of EMI and ERT techniques in predicting EC_e, the used data pairs were composed by predicted EC_e using ERT and predicted EC_e using EMI, ($pEC_{e\,ERT}$, $pEC_{e\,EMI}$), and were located at the position of the soil samples, as a result of the procedure for the calibrations development.

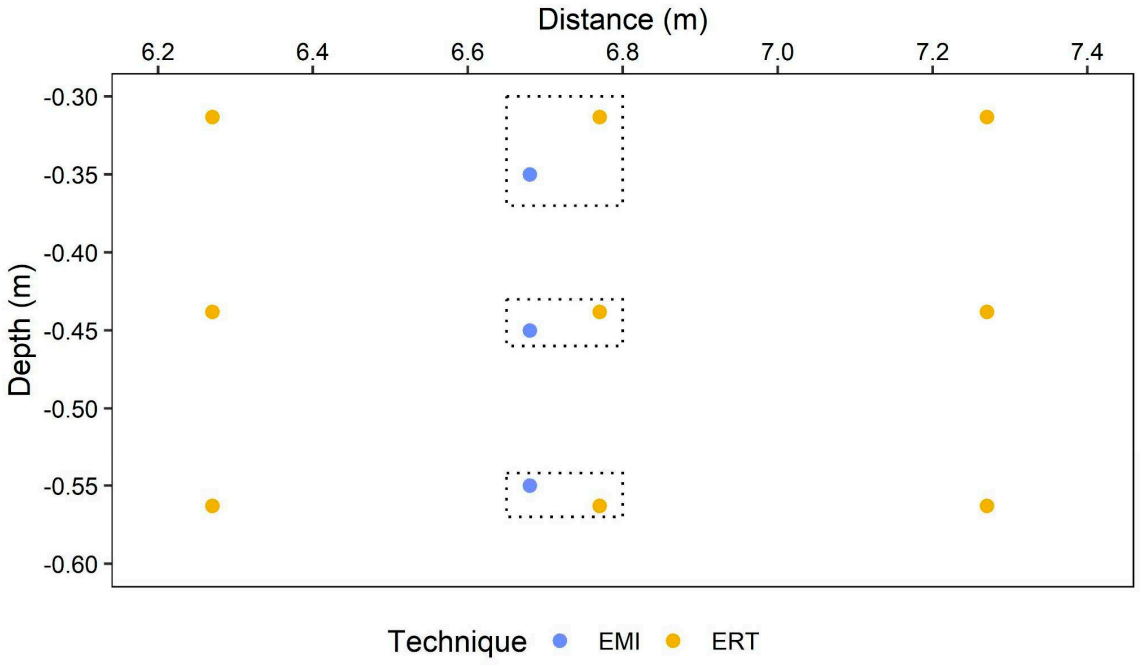

Figure 2. Comparison of electromagnetic induction (EMI) and electrical resistivity tomography (ERT) σ grids for location 1, Lezíria, Portugal.

Preprints (www.preprints.org) | NOT PEER-REVIEWED | Posted: 9 January 2024 doi:10.20944/preprints202401.0696.v1

To visualize the agreement of σ, data pairs were represented through σ_{EMI} against σ_{ERT} plots, and a modification of Bland-Altman plots (Bland & Altman, 1999). In the latter type of plot, the difference between each data pair value is plotted against the mean between the two values, which represents the most approximate value to the true value being studied (Bland & Altman, 1999). However, in this case, we used σ_{ERT} in the y-axis, as we considered it as σ reference and true value. A reference interval in which most differences between data fall is also included, and is called the 95% limits of agreement (Bland & Altman, 1999). The 95% limits of agreement can be calculated in different ways, depending on the differences between the data pairs values following a normal distribution or not (Bland & Altman, 1999), which was investigated using the qqPlot function of R language (R Core Team, 2020).

When the normal distribution of the differences between the data pairs values was verified, the 95% limits of agreement were calculated using the mean difference (MD) and the standard deviation (SD) of the differences as MD ± 1.96SD agreement (Bland & Altman, 1999). MD and SD were calculated according to the following equations:

$$MD = \frac{\sum_{i=1}^{n}\left(\sigma_{EMI_i} - \sigma_{ERT_i}\right)}{n} \quad (3)$$

$$SD = \sqrt{\frac{\sum_{i=1}^{n}\left(\sigma_{EMI_i} - \sigma_{ERT_i} - MD\right)^2}{n-1}} \quad (4)$$

When the normal distribution of the differences between the data pairs values was not verified, the 95% limits of agreement were defined using the median (MeD), the 5 percentile (p5), and the 95 percentile (p95) of the differences (Bland & Altman, 1999).

To visualize agreement between measured EC_e and predicted EC_e for each technique, data pairs were represented through another modification of the Bland-Altman plot, in which the difference between measured EC_e and predicted EC_e, for each technique, was plotted against the measured EC_e.

Spearman's rank correlation coefficient (RCC) between (i) the differences between σ_{ERT} and σ_{EMI}, and σ_{ERT}, for σ data; and (ii) the differences between measured EC_e and predicted EC_e, and the measured EC_e, for EC_e data, were calculated using SpearmanRho() function of R language (R Core Team, 2020). Spearman's RCC always returns a value placed between -1 and 1. In this case, it will indicate if the differences between the values being compared are related to the magnitude of the property being estimated. A Spearman's RCC closer to 1 means that the differences are very related to the magnitude of the property being estimated (Bland & Altman, 1999).

4. Results and discussion

4.1. Soil electrical conductivity obtained from EMI vs ERT

Figure 3 shows the 2D vertical σ models obtained by EMI and by ERT techniques for locations 1 to 4. For both techniques, a general increasing trend of σ is evident from the north to the south of the peninsula, accompanying the known soil salinity gradient, illustrating the strong correlation of σ with EC_e in the region, as verified previously in Farzamian et al., 2019; Paz et al., 2020a; b. Also, both techniques show that σ increases with depth at locations 2, 3, and 4, which correlates well with groundwater depth and salinity in these locations. However, this trend is not observed at location 1, possibly due to irrigation and deeper positioning of the saline groundwater at this site, making it less prone to capillary rise. Location 1 exhibits the lowest σ values, ranging from 50 to 160 mS m^{-1}, followed by slightly higher σ values at location 2 (i.e., 60-460 mS m^{-1}). Location 3 displays a greater variability in σ compared to the other two locations, featuring a minimum σ of 30 mS m^{-1} and a higher maximum of 530 mS m^{-1}. The σ gradient at location 4, however, is the most substantial, with an extreme maximum σ of over 1600 mS m^{-1}.

Preprints (www.preprints.org) | NOT PEER-REVIEWED | Posted: 9 January 2024 doi:10.20944/preprints202401.0696.v1

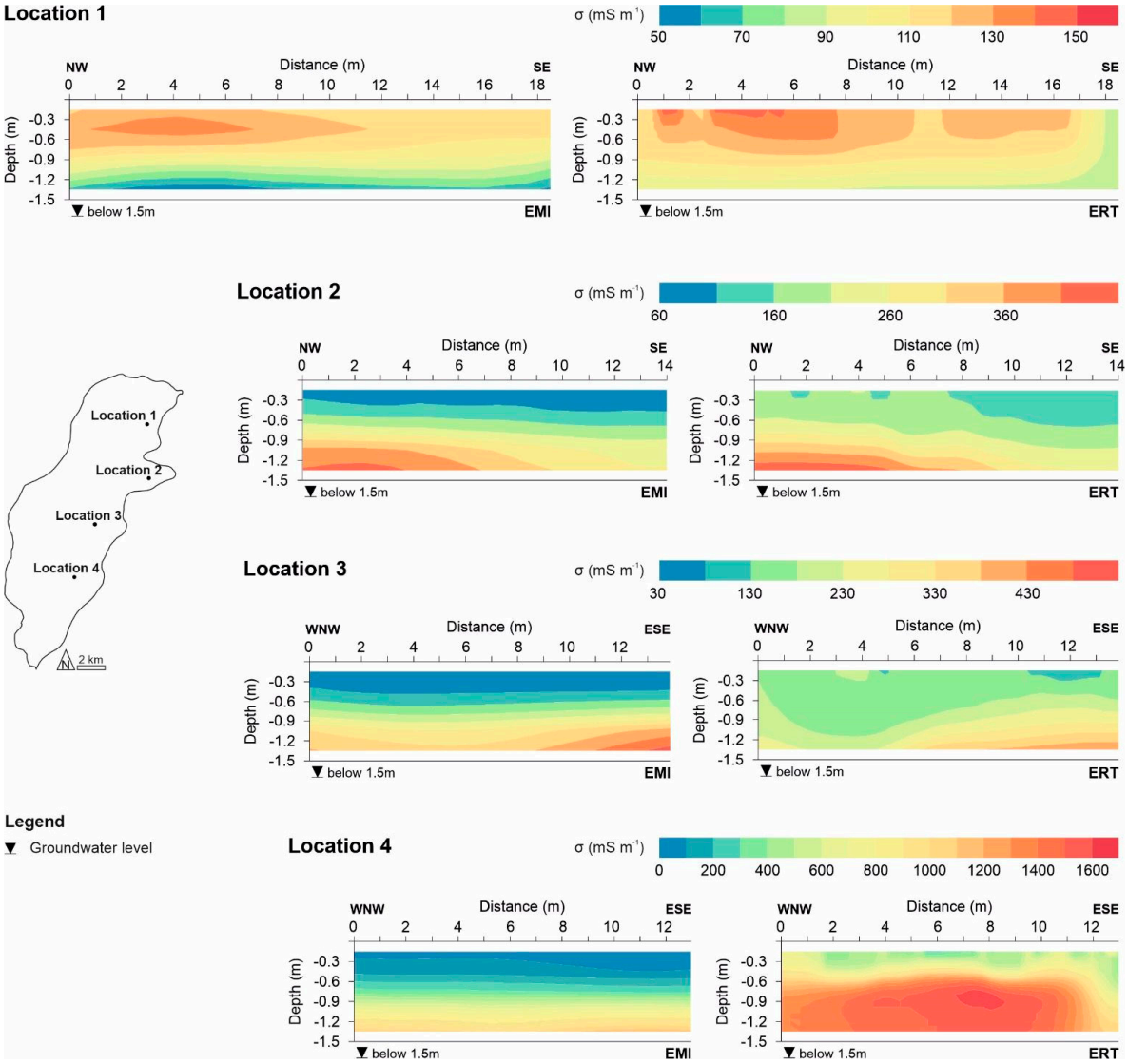

Figure 3. 2D vertical soil electrical conductivity (σ) models obtained from electromagnetic induction (EMI, left) and electrical resistivity tomography (ERT, right) techniques for locations 1 to 4.

To compare the EMI model with ERT, Figure 4 shows the plots that support the agreement analysis between EMI and ERT σ estimations. At location 1, a normal distribution of the differences between σ_{ERT} and σ_{EMI} data was verified, so the 95% limits of agreement were calculated using the mean difference (MD) and the standard deviation of the differences (SD), as explained in the methodology section. It can be verified that most differences between σ_{ERT} data and σ_{EMI} data fall in the -14.98 mS m^{-1} to 32.16 mS m^{-1} interval. The mean difference is 8.59 mS m^{-1}, and, since it's a positive value, indicates that, at this location, the EMI model tends to underestimate σ compared to the ERT model. This mean difference value is relatively low compared to the range of σ_{ERT} data (82.20–143.10 mS m^{-1}, Table 1). In terms of depths, agreement is generally good in topsoil (0–0.3 m), subsurface (0.3–0.6 m), and upper subsoil (0.6–0.9 m). However, the agreement diminishes in the intermediate subsoil (0.9–1.2 m), and lower subsoil (1.2–1.5 m), as evidenced by the distance of points to the 1:1 line in the σ_{EMI} against σ_{ERT} plot. Differences between σ_{EMI} and σ_{ERT} data in the topsoil, subsurface, and upper subsoil are the closest to the 0-horizontal line in the Bland-Altman plot. At this location, agreement increases with σ and decreases with depth. In comparison to the ERT model, there is an obvious tendency for the EMI model to underestimate σ in the lower subsoil (1.2–1.5 m). Spearman's RCC of -0.34, as observed in location 1, indicates that generally the differences between σ_{EMI} and σ_{ERT} are not related to the magnitude of σ.

Preprints (www.preprints.org) | NOT PEER-REVIEWED | Posted: 9 January 2024 doi:10.20944/preprints202401.0696.v1

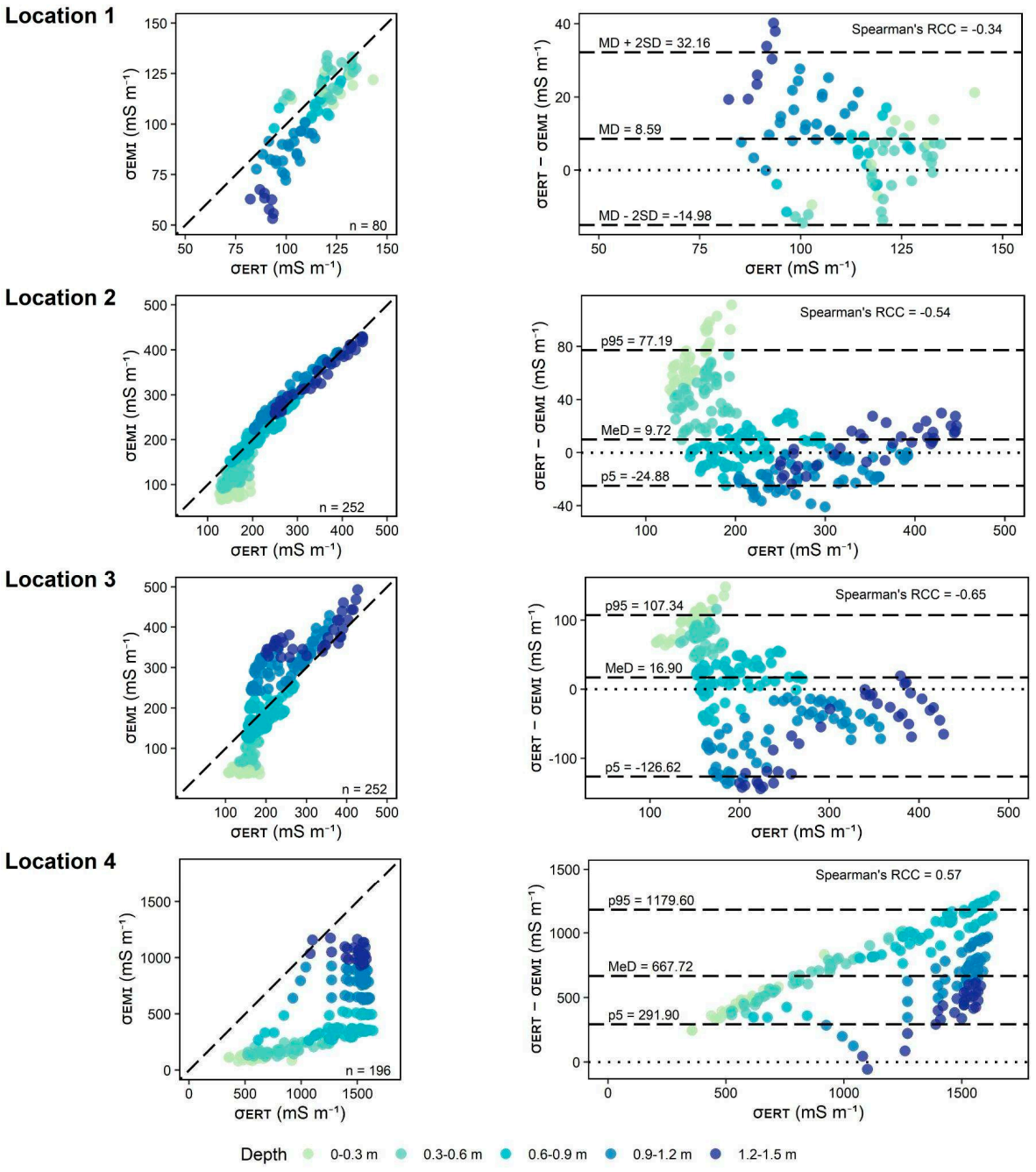

Figure 4. Agreement of soil electrical conductivity (σ) obtained from electromagnetic induction (EMI) and electrical resistivity tomography (ERT) techniques for locations 1 to 4: σ_{EMI} against σ_{ERT} plots with the 1:1 line (left), and modified Bland-Altman plots with the 95% limits of agreement (right). Plots include the number of data (n) (left), Spearman's rank correlation coefficient (RCC), mean difference (MD), standard deviation (SD), median (MeD), the 5 percentile (p5), and the 95 percentile (p95) (right).

Table 1. Statistics of Soil electrical conductivity obtained from electrical resistivity tomography (σ_{ERT}), and measured soil salinity (mEC_e): minimum, maximum, range, and number of data, at locations 1 to 4 and at all locations together, respectively.

	Unit	Location	Minimum	Maximum	Range	Number of data
σ_{ERT}	mS m^{-1}	1	82.20	143.10	60.90	80
		2	126.70	446.20	319.50	252
		3	107.40	427.50	320.10	252

		4	356.40	1640.00	1283.60	196
mEC_e	dS m^{-1}	all	0.75	37.10	36.75	19

σ_{ERT} is soil electrical conductivity obtained by electrical resistivity tomography, mEC_e is measured soil salinity obtained from saturated soil paste extract (ECe).

At locations 2 to 4, a normal distribution of the differences between σ_{EMI} and σ_{ERT} data was not verified, so the 95% limits of agreement were calculated using the median (MeD), the 5 percentile (p5), and the 95 percentile (p95) of the differences (see section 2.4).

At location 2, most differences between σ_{ERT} and σ_{EMI} data fall in the -24.88 mS m^{-1} to 77.19 mS m^{-1} interval. The median is 9.72 mS m^{-1}, which indicates that, in general, at this location EMI model similarly tends to underestimate σ, compared to the ERT model. Also, this value is low compared to the range of σ_{ERT} data (126.70–446.20 mS m^{-1}, Table 1). In terms of depths, agreement is generally good in the upper subsoil (0.6–0.9 m) and lower subsoil (1.2–1.5 m), which can be verified by the distance of points to the 1:1 line in the σ_{EMI} against σ_{ERT} plot. Also, differences between σ_{EMI} data and σ_{ERT} data in the upper and lower subsoil are the closest to the 0-horizontal line in the Bland-Altman plot. At this location, agreement increases with σ and with depth. This contrasts with the observations at location 1, where the most significant disagreement was noted in the lower subsoil (1.2–1.5 m). However, the distribution of σ at location 1 differs significantly from the variability observed in the other three locations, as σ decreases with depth at location 1. Spearman's RCC of -0.54 indicates that generally, the differences between σ_{EMI} and σ_{ERT} tend to slightly decrease when σ increases.

At location 3, most of the differences between σ_{ERT} and σ_{EMI} data fall in the -126.62 mS m^{-1} to 107.34 mS m^{-1} interval. The median is 16.90 mS m^{-1}, which indicates that, similarly to locations 1 and 2, and in general, at this location EMI model tends to underestimate σ, compared to the ERT model. Also, this value is low compared to the range of σ_{ERT} data (107.40–427.50 mS m^{-1}, Table 1). In terms of depths, agreement is generally good in the subsurface (0.3–0.6 m), and upper subsoil (0.6–0.9 m), as evidenced by the proximity of points to the 1:1 line in the σ_{EMI} against σ_{ERT} plot and to the 0-horizontal line in the Bland-Altman plot. Spearman's RCC of -0.65 indicates that the differences between σ_{EMI} and σ_{ERT} slightly decrease when σ increases.

At location 4, most differences between σ_{ERT} and σ_{EMI} data fall in the 291.90 mS m^{-1} to 1179.60 mS m^{-1} interval. This interval is totally above the 0-horizontal line in the Bland-Altman plot, which, together with a median of 667.72 mS m^{-1}, indicates that at this location, the EMI model tends to drastically underestimate σ, compared to the ERT model. Also, this value is significantly high, in the range of σ_{ERT} data (356.40–1640.00 mS m^{-1}, Table 1). In terms of depths, there is no significant agreement between σ_{ERT} and σ_{EMI}, as evidenced by the lack of proximity of points to the 1:1 line in the σ_{EMI} against the σ_{ERT} plot and to the 0-horizontal line in the Bland-Altman plot. Spearman's RCC of 0.57 indicates that the differences between σ_{EMI} and σ_{ERT} slightly increase when σ increases.

Comparing the results between locations suggests that the EMI models tend to underestimate σ when compared to the ERT models in all four locations. However, in locations 1,2, and 3, with σ variability inferred from the ERT model in the 50-500 mS m^{-1} range, the underestimation of the EMI model was not significant, suggesting that, the obtained EMI models are in good and acceptable agreement with those inferred from detailed ERT investigation. This is not the case at location 4, as the underestimation tendency was quite drastic at this location where the σ variability inferred from the ERT model falls in the range of 500-1600 mS m^{-1}. This is likely linked to the relationship between the quadrature component of the EMI signal and σ in superconductive soil at location 4, which may exhibit a non-monotonic behavior (McLachlan et al., 2020). In such situations, obtaining more representative EC_a values may need the use of both the in-phase and quadrature components of the EMI signal (Guillemoteau et al., 2015). However, the in-phase component has to be adequately calibrated, as it is susceptible to signal instability and offsets (De Smedt et al., 2016), which was not considered in this study. This presents a significant challenge when estimating σ in highly saline soil, where conductivity is anticipated to be extremely high. In this context, the robust EC_a estimation approach, proposed by (Hanssens et al. 2019) may enhance the reliability of EC_a estimation over

Preprints (www.preprints.org) | NOT PEER-REVIEWED | Posted: 9 January 2024 doi:10.20944/preprints202401.0696.v1

superconductive areas. Alternatively, ERT (e.g., von Hebel et al., 2019) or TDR (Dragonetti et al., 2018) measurements carried out along the same transects can be used to calibrate EC_a data to obtain more representative EC_a values.

4.2. Soil salinity obtained from EMI vs ERT

Figure 5 shows the two regional regression models that were developed to predict EC_e, one using the σ obtained from the inversion of EMI data and the other using σ, obtained from the inversion of ERT, and their prediction results. Both models have a strong R^2, with EMI (0.86) being higher than ERT (0.75). The leave-one-out cross-validation resulted in acceptable and comparable RMSE and ME. Obtained RMSE of 3.96 dS m^{-1} for EMI, and of 4.72 dS m^{-1} for ERT, are low in the measured EC_e range (0.75–37.1 dS m^{-1}, Table 1) and comparable between them. ME of 3.22 dS m^{-1} for EMI, and 2.32 dS m^{-1} for ERT, means comparable underestimation of the predicted data for both techniques.

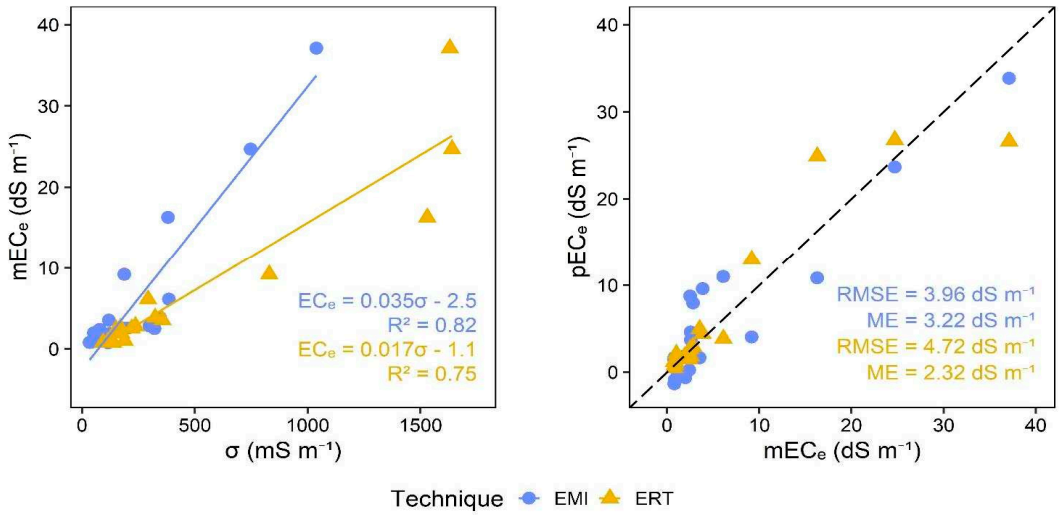

Figure 5. Measured soil salinity (mEC_e) versus soil electrical conductivity (σ) obtained from electromagnetic induction (EMI) and electrical resistivity tomography (ERT) techniques for the regional regression models (left), and predicted soil salinity (pEC_e) obtained from the leave-one-out-cross-validation of the regression models (right). Plots include regression models and their coefficient of determination (R^2) (left), and their root mean square error (RMSE) and mean error (ME).

Figure 6 shows the plot of the differences between measured EC_e and predicted EC_e, for each technique, against the measured EC_e. The proximity of the points to the 0-horizontal line indicates that there is good agreement between measured and predicted EC_e. Points above the line indicate underestimation, while points below the line indicate overestimation. In the non-saline classification interval of soil salinity, both techniques showed good agreement between measured and predicted EC_e. In the slightly saline classification interval, EMI provided mostly overestimated predictions but also some underestimated predictions, whereas ERT showed good agreement between measured and predicted EC_e. In the moderately saline classification interval, EMI provided one overestimated prediction, while ERT underestimated that same EC_e measurement. In the very saline classification interval, EMI provided one underestimated prediction, while ERT overestimated that same EC_e measurement. In the highly saline classification interval, the same happened as in the previous interval, except for one EC_e measurement, which was underestimated by both techniques, but still is classified as highly saline, for both techniques. Spearman's RCC calculated for EMI (0.24), indicates that there is an underestimation tendency as the magnitude of EC_e (soil salinity) increases. In the case of ERT, Spearman's RCC of –0.12 indicates a slight overestimation tendency as the soil salinity grows.

A thorough examination of the regression models reveals that, despite the EMI model significantly underestimating σ in the superconductive zone at location 4, resulting in a distinct

Preprints (www.preprints.org) | NOT PEER-REVIEWED | Posted: 9 January 2024 doi:10.20944/preprints202401.0696.v1

regression linear slope between EC_e and σ (EMI vs. ERT), this issue has not adversely affected the overall predictive capability of the regional calibration when compared to the results obtained from ERT. This is attributed to the fact that, although EMI underestimated σ at location 4, the pattern of σ distribution and its variations with depth align with those obtained from the ERT model.

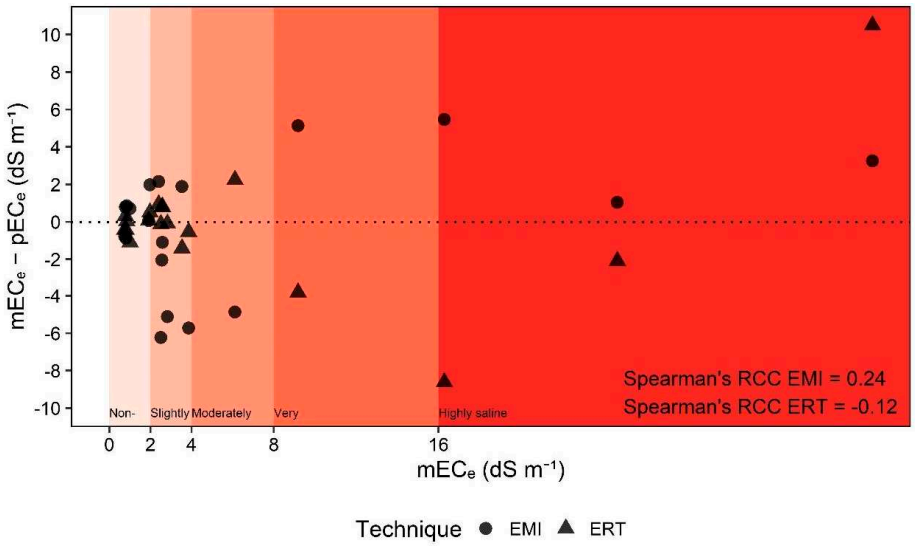

Figure 6. Agreement of measured soil salinity (mECe) and predicted soil salinity (pECe) obtained by electromagnetic induction (EMI) and electrical resistivity tomography (ERT) techniques, with Spearman's rank correlation coefficient (RCC).

To provide a better insight into the prediction ability of both methodologies in different locations, Figure 7 depicts the 2D vertical maps of soil salinity classification obtained from the conversion of σ obtained by EMI and ERT for locations 1 to 4, using the corresponding calibration. The filled circles in the maps represent the position and classification of the soil samples (measured EC_e).

Preprints (www.preprints.org) | NOT PEER-REVIEWED | Posted: 9 January 2024 doi:10.20944/preprints202401.0696.v1

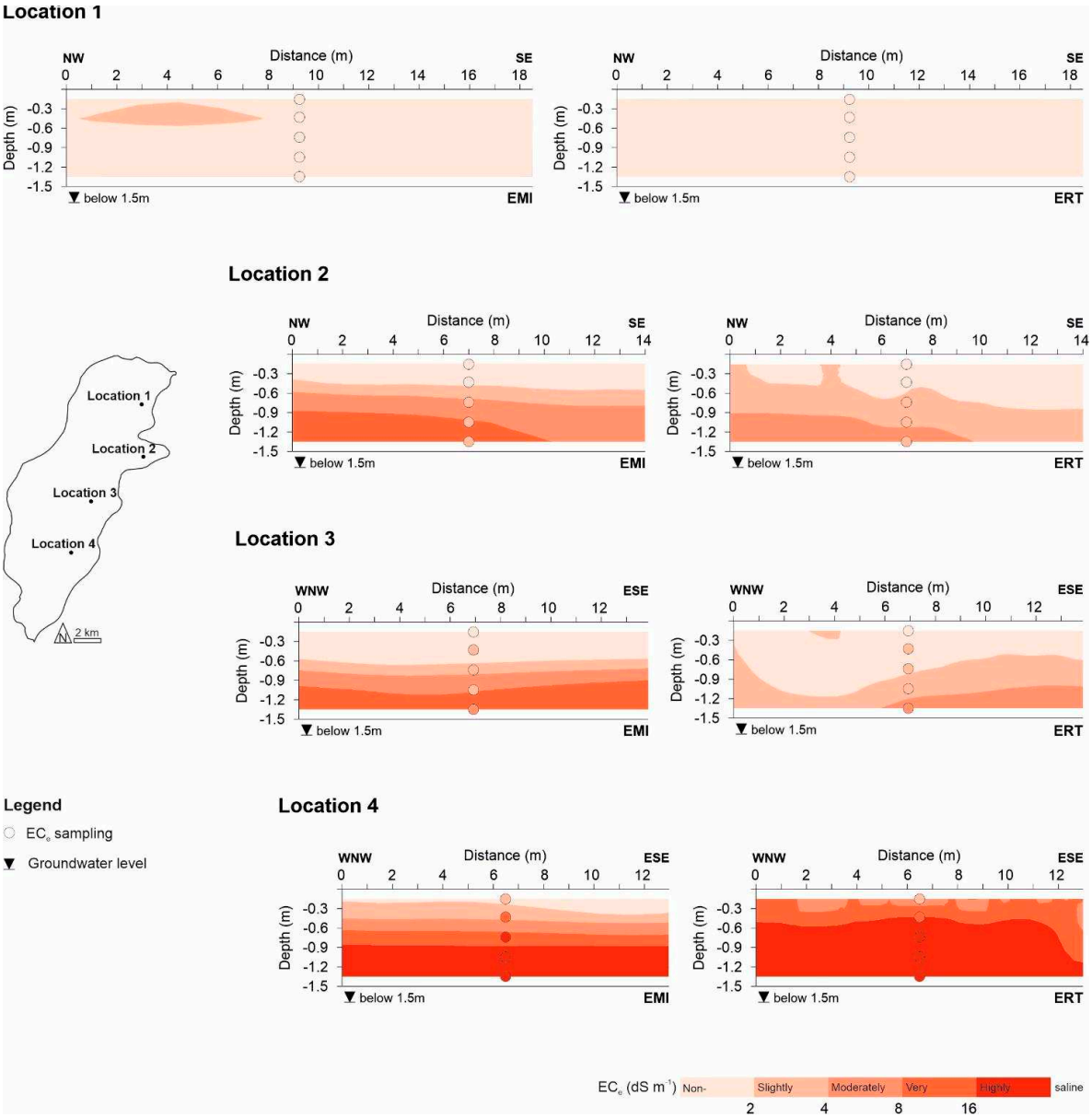

Figure 7. 2D vertical soil salinity classification maps obtained by electromagnetic induction (EMI, left) and electrical resistivity tomography (ERT, right) techniques for locations 1 to 4. The filled circles represent the position and classification of the soil samples (measured EC_e).

At location 1 there is total agreement between the predicted classification and the actual classification obtained from the samples, for both techniques. At location 2 soil salinity is overestimated by EMI at intermediate (0.9–1.2 m) and lower subsoil (1.2–1.5 m), while it is also overestimated by ERT but only at the lower subsoil (1.2–1.5 m). At location 3 soil salinity is underestimated by EMI at subsurface (0.3–0.9 m) and overestimated at intermediate (0.9–1.2 m) and lower subsoil (1.2–1.5 m), while it is underestimated by ERT at subsurface (0.3–0.9 m) and upper subsoil (0.6–0.9 m). At location 4 soil salinity is underestimated by EMI from topsoil to upper subsoil (0–0.9 m), while there is total agreement between the predicted classification and the actual classification by ERT.

As anticipated, the salinity maps obtained from EMI and ERT are acceptably comparable, although EMI generally underestimated σ. Both methods displayed similar levels of underestimations and overestimations, indicating a comparable level of prediction accuracy. The underestimation or overestimation of soil salinity based on σ is not only related to the geophysical approach but also influenced by the variability of other soil properties along the transects, such as

 doi:10.20944/preprints202401.0696.v1

soil texture, moisture content, and temperature. These factors collectively affect soil electrical conductivity, making it challenging to accurately predict soil salinity solely from σ (Farzamian et al., 2019; Paz et al., 2020a).

5. Conclusion

In this study, EMI and ERT surveys, and soil sampling were carried out at four locations with different salinity levels across the study area of Lezíria de Vila Franca, in dry season conditions, to analyse the agreement between the two techniques in estimating soil electrical conductivity and compare their ability in predicting soil salinity. While ERT may not offer a precise subsurface conductivity distribution of the subsoil (as no indirect method can achieve that), it stands out as one of the most reliable techniques for imaging the subsurface conductivity distribution. Conversely, EMI measurements are highly sensitive to various factors, including ground coupling, thermal drifts, and EM noise. Hence, it is sensible to consider an ERT inversion as a reference model that the EMI inversion should strive to approximate.

Based on the obtained results in this experiment, there was a reasonable agreement between the EMI and ERT models in three locations, where σ ranged from 50 to 500 mS m^{-1}. In contrast, at location 4, where σ surpassed 1000 mS m^{-1}, EMI notably underestimated σ in comparison to ERT. However, EMI models could still well predict the increasing trend of σ with depth. This suggests that the obtained EMI model may substantially underestimate σ in an extremely saline area given the very high level of soil conductivity which exhibits a non-monotonic relationship between the quadrature component of the EMI signal. Under this condition, the σ values inferred from EMI modelling cannot be used alone to assess the soil salinity level without a site-specific regression or applying a more robust approach to obtain a more representative EC_a value (Hanssens et al. 2019; von Hebel et al., 2019; Dragonetti et al., 2018). Further case studies across different soil types and salinity levels will offer more insights into the circumstances under which EMI performs optimally.

The regional regression models based on both EMI and ERT demonstrated similar predictive capabilities. Despite the EMI model significantly underestimating σ in the superconductive zone at location 4, leading to a distinct regression linear slope between EC_e and σ, this issue did not markedly affect the overall predictive performance of the regional calibration when compared to the results from ERT. This is because despite the underestimation of σ by EMI at location 4, the distribution pattern and depth-related variations of σ similarly mirrored those obtained from the ERT model, resulting in comparable prediction abilities. Nevertheless, additional case studies across areas with high conductivities are necessary to further evaluate this observation. Specifically, EMI vs ERT studies across sites with inverted soil salinity, where there is a superconductive zone over a more resistive zone, are particularly needed to assess the prediction ability of EMI in contrasting conditions, compared to this study.

Author Contributions: Conceptualization, Maria Paz and Mohammad Farzamian; Data curation, Nádia Luísa Castanheira and Mohammad Farzamian; Formal analysis, Maria Paz and Mohammad Farzamian; Funding acquisition, Maria Gonçalves and Fernando Monteiro Santos; Investigation, Maria Paz, Nádia Luísa Castanheira, Ana Marta Paz, Maria Gonçalves and Mohammad Farzamian; Methodology, Maria Paz, Ana Marta Paz, Fernando Monteiro Santos and Mohammad Farzamian; Project administration, Maria Gonçalves, Fernando Monteiro Santos and Mohammad Farzamian; Resources, Nádia Luísa Castanheira, Ana Marta Paz and Maria Gonçalves; Software, Fernando Monteiro Santos; Supervision, Maria Gonçalves and Mohammad Farzamian; Validation, Maria Paz and Mohammad Farzamian; Visualization, Maria Paz; Writing – original draft, Maria Paz and Mohammad Farzamian; Writing – review & editing, Maria Paz, Nádia Luísa Castanheira, Ana Marta Paz, Maria Gonçalves, Fernando Monteiro Santos and Mohammad Farzamian.

Funding: This work was funded by the Portuguese research agency, Fundação para a Ciência e a Tecnologia (FCT), in the scope of project SALTFREE – ARIMNET2/0004/2015 SALTFREE and ARIMNET2/0005/2015

SALTFREE. This work was also supported by the European Joint Programme Cofund on Agricultural Soil Management (EJP SOIL grant number 862695), funded by the European Union's Horizon H2020 research and innovation and was carried out in the framework of the STEROPES of EJP-SOIL.

Acknowledgments: The authors express their appreciation to the Associação de Beneficiários da Lezíria Grande de Vila Franca de Xira for granting access to study sites and their ongoing support. Special thanks are also extended to Manuel Fernandes and Fernando Pires from INIAV for their field assistance. This work was funded by the Portuguese Fundação para a Ciência e a Tecnologia (FCT) I.P./MCTES through national funds (PIDDAC) – UIDB/50019/2020 (https://doi.org/10.54499/UIDB/50019/2020), UIDP/50019/2020 (https://doi.org/10.54499/UIDP/50019/2020) and LA/P/0068/2020 (https://doi.org/10.54499/LA/P/0068/2020).

References

1. Allison, L. E., Bernstein, L., Bower, C. A., Brown, J. W., Fireman, M., Hatcher, J. T., Hayward, H. E., Pearson, G. A., Reeve, R. C., Richards, L. A., & Wilcox, L. v. (1954). *Diagnosis and Improvement of Saline Alkali Soils, Agricultural Handbook* (L. A. Richards (ed.)). United States Department of Agriculture. https://www.ars.usda.gov/ARSUserFiles/20360500/hb60_pdf/hb60complete.pdf
2. Araújo, O.S., Picotti, S., Francese, R.G., Bocchia, F., Santos, F. A. M., Giorgi, M., & Tessarollo, A. (2023). Frequency domain electromagnetic calibration for improved detection of sand intrusions in river embankments. *Leading Edge*, 42(9), 615-624. https://doi.org/10.1190/tle42090615.1
3. Barrett-Lennard, E., Bennett, S., & Colmer, T. (2008). Standardising terminology for describing the level of salinity in soils in Australia. *2nd International Salinity Forum. Salinity, Water and Society: Global Issues, Local Action*.
4. Blanchy, G., Saneiyan, S., Boyd, J., McLachlan, P., & Binley, A. (2020). ResIPy, an intuitive open source software for complex geoelectrical inversion/modeling, *Computers & Geosciences*, 137, 104423, https://doi.org/10.1016/j.cageo.2020.104423
5. Bland, J. M., & Altman, D. G. (1999). Measuring agreement in method comparison studies. *Statistical Methods in Medical Research*, *8*(2), 135–160. https://doi.org/10.1177/096228029900800204
6. Corwin, D. L., & Lesch, S. M. (2005). Apparent soil electrical conductivity measurements in agriculture. *Computers and Electronics in Agriculture*, *46*, 11–43. https://doi.org/10.1016/j.compag.2004.10.005
7. deGroot-Hedlin, C., & Constable, S. (1990). Occam's inversion to generate smooth, two-dimensional models from magnetotelluric data. *GEOPHYSICS*, *55*(12), 1613–1624. https://doi.org/10.1190/1.1442813
8. De Smedt, P., Delefortrie, S., & Wyffels, F., (2016). Identifying and removing micro-drift in ground-based electromagnetic induction data, *Journal of Applied Geophysics*, 131, 14–22, https://doi.org/10.1016/j.jappgeo.2016.05.004
9. Dragonetti, G., Comegna, A., Ajeel, A., Deidda, G. P., Lamaddalena, N., Rodriguez, G., Vignoli, G., & Coppola, A. (2018). Calibrating electromagnetic induction conductivities with time-domain reflectometry measurements, *Hydrology and Earth System Sciences*, 22, 1509–1523, https://doi.org/10.5194/hess-22-1509-2018, 2018.
10. Dragonetti, G., Farzamian, M., Basile, A., Monteiro Santos, F. & Coppola, A. (2022). In-situ estimation of soil hydraulic and hydrodispersive properties by inversion of Electromagnetic Induction measurements and soil hydrological modeling, *Hydrology and Earth System Sciences*, *26*, *5119–5136*, https://doi.org/10.5194/hess-26-5119-2022.
11. EMTOMO. 2018. EMTOMO manual for EM4Soil: A program for 1-D laterally constrained inversion of EM data. EMTOMO, Lisbon, Portugal.
12. Farzamian, M., Paz, M. C., Paz, A. M., Castanheira, N. L., Gonçalves, M. C., Monteiro Santos, F. A., & Triantafilis, J. (2019). Mapping soil salinity using electromagnetic conductivity imaging—A comparison of regional and location-specific calibrations. *Land Degradation and Development*, *30*(12). https://doi.org/10.1002/ldr.3317
13. Farzamian, M, Autovino, D., Basile, A., De Mascellis, R., Dragonetti, G., Monteiro Santos, F., Binley, A., & Coppola, A. (2021). Assessing the dynamics of soil salinity with time-lapse inversion of electromagnetic data guided by hydrological modelling. *Hydrology and Earth System Sciences*, 25(3), 1509–1527. https://doi.org/10.5194/hess-25-1509-2021
14. Farzamian, M., Bouksila, F., Paz, A. M., Monitero Santos, F. M., Zemni, N., Slama, F., Ben Silmane, A., Selim, T., & Triantafilis, J. (2023). Landscape-scale mapping of soil salinity with multi-height electromagnetic induction and quasi-3d inversion in Saharan Oasis, Tunisia. *Agricultural Water Management*, 284, 108330. https://doi.org/10.1016/j.agwat.2023.108330
15. Fischer, G., Nachtergaele, F. O., Prieler, S., Teixeira, E., Toth, G., van Velthuizen, H., Verelst, L., & Wiberg, D. (2012). *Global Agro-ecological Zones (GAEZ v3.0) - Model Documentation*. IIASA, Laxenburg, Austria and FAO, Rome, Italy. http://www.fao.org/soils-portal/soil-survey/soil-maps-and-databases/harmonized-world-soil-database-v12/en/

16. Guillemoteau, J., Sailhac, P., Boulanger, C., & Trules, J. (2015). Inversion of ground constant offset loop-loop electromagnetic data for a large range of induction numbers. *Geophysics,* 80 (1), E11–E21. https://doi.org/10.1190/geo2014-0005.1
17. Hanssens, D., Delefortrie, S., Bobe, C., Hermans, T., & De Smedt, P. (2019). Improving the reliability of soil EC-mapping: robust apparent electrical conductivity (RECa) estimation in ground-based frequency domain electromagnetics. *Geoderma,* 337, 1155–1163. https://doi.org/10.1016/j.geoderma.2018.11.030
18. Huang, J., Lark, R. M., Robinson, D. A., Lebron, I., Keith, A. M., Rawlins, B., Tye, A., Kuras, O., Raines, M., & Triantafilis, J. (2014). Scope to predict soil properties at within-field scale from small samples using proximally sensed γ-ray spectrometer and EM induction data, *Geoderma*, 232-234, 69 - 80, http://dx.doi.org/10.1016/j.geoderma.2014.04.031
19. Jupp, D. L. B., & Vozoff, K. (1975). Stable Iterative Methods for the Inversion of Geophysical Data. *Geophysical Journal of the Royal Astronomical Society*, *42*(3), 957–976. https://doi.org/10.1111/j.1365-246X.1975.tb06461.x
20. Kaufman, A., & Keller, G. V. (1984). Frequency and Transient Sounding Methods in Geochemistry and Geophysics, Vol. 16 A, A. Kaufman and G. V. Keller, Elsevier, Amsterdam, 1983 686 pp., £85.55/\ \$144.75. *Geophysical Journal International*, *77*(3), 935–937. https://doi.org/10.1111/j.1365-246X.1984.tb02230.x
21. Khongnawang, T., Zare, E., Srihabun, P., Khunthong, I., & Triantafilis, J. (2022). Digital soil mapping of soil salinity using EM38 and quasi-3d modeling software (EM4Soil), *Soil Use and Management*, 38, 277 - 291, http://dx.doi.org/10.1111/sum.12778
22. Koganti, T., Narjary, B., Zare, E., Pathan, A. L., Huang, J., & Triantafilis, J. (2018). Quantitative mapping of soil salinity using the DUALEM-21S instrument and EM inversion software, *Land Degradation and Development*, 29, 1768 - 1781, http://dx.doi.org/10.1002/ldr.2973
23. Lavou´e, F., Van Der Kruk, J., Rings, J., Andr´e, F., Moghadas, D., Huisman, J.A., Lambot, S., Weihermüller, L., Vanderborght, J., & Vereecken, H. (2010). Electromagnetic induction calibration using apparent electrical conductivity modelling based on electrical resistivity tomography. *Near Surface Geophysics,* 8 (6), 553–561, https://doi.org/10.3997/1873-0604.2010037
24. Loke, M. H. (2002). Tutorial: 2D and 3D Electrical Imaging Surveys, Technical Note, 2nd edn., Geotomo Software, Malaysia.
25. McLachlan, P., Blanchy, G., & Binley, A. (2021). EMagPy: open-source standalone software for processing, forward modeling and inversion of electromagnetic induction data. *Computer and Geoscience*, 146, 104561 https://doi.org/10.1016/j.cageo.2020.104561.
26. Minsley, B.J., Smith, B.D., Hammack, R., Sams, J.I., & Veloski, G. (2012). Calibration and filtering strategies for frequency domain electromagnetic data. *Journal of Applied Geophysics*, 80, 56–66, https://doi.org/10.1016/j.jappgeo.2012.01.008
27. Moghadas, D., Jadoon, K., & McCabe, M. (2017). Spatiotemporal monitoring of soil water content profiles in an irrigated field using probabilistic inversion of time-lapse EMI data. *Advanced in Water Resources,* 110 https://doi.org/10.1016/j.advwatres.2017.10.019.
28. Moghadas, D. (2019). Probabilistic inversion of multiconfiguration electromagnetic induction data 863 using dimensionality reduction technique: a numerical study. *Vadose Zone* Journal, 18, 1–16. https://doi.org/10.2136/vzj2018.09.0183.
29. Monteiro Santos, F. A. (2004). 1-D laterally constrained inversion of EM34 profiling data. *Journal of Applied Geophysics*, *56*(2). https://doi.org/10.1016/j.jappgeo.2004.04.005
30. Monteiro Santos, F., Triantafilis, J., & Bruzgulis, K. (2011). A spatially constrained 1D inversion algorithm for quasi-3D conductivity imaging: Application to DUALEM-421 data collected in a riverine plain. *Geophysics*, *76*. https://doi.org/10.1190/1.3537834
31. Narciso, J., Bobe, C., Azevedo, L., & Van De Vijver, E. (2022). A comparison between Kalman ensemble generator and geostatistical frequency-domain electromagnetic inversion: the impacts on near-surface characterization. *Geophysics* 87 (5), E335–E346. https://doi.org/10.1190/geo2021-0498.1.
32. Paz, Ana Marta, Esperanza Amezketa, Loredana Canfora, Nadia Castanheira, Gloria Falsone, Maria C. Gonçalves, Ian Gould, et al. (2023). Salt-Affected Soils: Field-Scale Strategies for Prevention, Mitigation, and Adaptation to Salt Accumulation. *Italian Journal of Agronomy* 18 (2). https://doi.org/10.4081/ija.2023.2166.
33. Paz, M. C., Farzamian, M., Paz, A. M., Castanheira, N. L., Gonçalves, M. C., & Santos, F. M. (2020a). Assessing soil salinity dynamics using time-lapse electromagnetic conductivity imaging. *SOIL*, *6*(2). https://doi.org/10.5194/soil-6-499-2020
34. Paz, A. M., Castanheira, N., Farzamian, M., Paz, M. C., Gonçalves, M. C., Monteiro Santos, F. A., & Triantafilis, J. (2020b). Prediction of soil salinity and sodicity using electromagnetic conductivity imaging. *Geoderma*, *361*. https://doi.org/10.1016/j.geoderma.2019.114086
35. R Core Team. (2020). *R: A language and environment for statistical computing.* R Foundation for Statistical Computing, Vienna. https://www.r-project.org/

36. Ramos T. B., Castanheira N., Oliveira A. R., Paz A. M., Darouich H., Simionesei L., et al. (2020). Soil salinity assessment using vegetation indices derived from sentinel-2 multispectral data. application to lezíria grande, Portugal. *Agricultural Water Management,* 241, 106387, https://doi.org/10.1016/j.agwat.2020.106387.
37. Robinet, J., von Hebel, C., Govers, G., van der Kruk, J., Minella, J. P. G., Schlesner, A., Ameijeiras-Mariño, Y., & Vanderborght, J. (2018). Spatial variability of soil water content and soil electrical conductivity across scales derived from Electromagnetic Induction and Time Domain Reflectometry. *Geoderma*, *314*, 160–174. https://doi.org/10.1016/j.geoderma.2017.10.045
38. Rücker, C., Günther, T., & Wagner, F. M. (2017). pyGIMLi: An open-source library for modelling and inversion in geophysics. *Computers and Geosciences*, *109*(July), 106–123. https://doi.org/10.1016/j.cageo.2017.07.011
39. Shanahan, P. W., Binley, A., Whalley, W. R., & Watts, C. W. (2015). The Use of Electromagnetic Induction to Monitor Changes in Soil Moisture Profiles Beneath Different Wheat Genotypes, *Soil Science Society of America Journal*, 79, 459–466, https://doi.org/10.2136/sssaj2014.09.0360.
40. Triantafilis, J. (2009). Field level digital soil mapping of cation exchange capacity using electromagnetic induction and a hierarchical spatial regression model, *Australian Journal of Soil Research*, 47, 651 - 663, http://dx.doi.org/10.1071/SR08240
41. von Hebel, C., Rudolph, S., Mester, A., Huisman, J. A., Kumbhar, P., Vereecken, H., & van der Kruk, J. (2014). Three-dimensional imaging of subsurface structural patterns using quantitative large-scale multiconfiguration electromagnetic induction data, *Water Resource Research*, 50, 2732–2748, https://doi.org/10.1002/2013WR014864
42. Von Hebel, C., Van Der Kruk, J., Huisman, J. A., Mester, A., Altdorff, D., Endres, A. L., Zimmermann, E., Garré, S., & Vereecken, H. (2019). Calibration, Conversion, and Quantitative Multi-Layer Inversion of Multi-Coil Rigid-Boom Electromagnetic Induction Data. *Sensors, 19, Page 4753*, *19*(21), 4753. https://doi.org/10.3390/S19214753
43. Whalley, W. R., Binley, A. M., Watts, C. W., Shanahan, P., Dodd, I. C., Ober, E. S., Ashton, R. W., Webster, C. P., White, R. P., & Hawkesford, M. J. (2017). Methods to estimate changes in soil water for phenotyping root activity in the field, Plant Soil, 415, 407–422, https://doi.org/10.1007/s11104-016-3161-1
44. Zare, E., Li, N., Khongnawang. T., Farzamian, M., & Triantafilis, J. (2020). Identifying potential leakage zones in an irrigation supply channel by mapping soil properties using electromagnetic induction, inversion modelling and a support vector machine, *Soil Systems*, 4, 1 - 18, http://dx.doi.org/10.3390/soilsystems4020025
45. Zhao, D., Li, N., Zare, E., Wang, J., & Triantafilis, J. (2020). Mapping cation exchange capacity using a quasi-3d joint inversion of EM38 and EM31 data, *Soil and Tillage Research*, 200, http://dx.doi.org/10.1016/j.still.2020.104618
46. Zhao, X., Wang, J., Zhao, D., Sefton, M., & Triantafilis J. (2022). Mapping Cation Exchange Capacity (CEC) Across Sugarcane Fields with Different Comparisons by Using DUALEM Data, *Journal of Environmental and Engineering Geophysics*, 27, pp. 191 - 205, http://dx.doi.org/10.32389/jeeg22-002